

Strong-field below-threshold harmonic generation

Dylan C. Yost, Thomas R. Schibli, Jun Ye

*JILA, National Institute of Standards and Technology, and University of Colorado.
Department of Physics, University of Colorado, Boulder, Colorado 80309-0440*

Jennifer L. Tate, James Hostetter, Kenneth J. Schafer, Mette B. Gaarde

Department of Physics and Astronomy, Louisiana State University, Baton Rouge, Louisiana 70803-4001

We present experimental and theoretical evidence that both multiphoton and tunneling initiated processes contribute to the generation of below-threshold harmonics in xenon. The measured yield of these low order harmonics exhibits interferences as a function of the 1070 nm laser intensity, and their far-field spatial distributions contain both on-axis and off-axis contributions. Our theoretical analysis shows that the interference results from the presence of multiple generation pathways, and that the off-axis radiation is due to a contribution with a strongly intensity-dependent dipole phase. This dipole phase originates in semi-classical laser-driven continuum dynamics, in analogy with above-threshold harmonic generation.

PACS numbers: 42.65.Ky, 42.65.Re, 32.80.Rm

Steady progress in strong-field atomic physics has paved the way for the study of high harmonic generation (HG), strong-field ionization and recently, the probing of matter on attosecond time scales [1, 2, 3, 4]. In parallel, the advent of frequency comb technology has found powerful applications in coherent control, precision spectroscopy and arbitrary waveform generation [5, 6, 7]. Intriguingly, these disciplines may merge in the development of direct frequency comb spectroscopy and coherent control at extreme ultraviolet (XUV) wavelengths [8, 9]. The enabling technology lies in the recent demonstrations of high harmonic generation at very high repetition frequencies (~ 100 MHz) [10, 11]. The high repetition rate not only increases the average power of the harmonics, but also helps maintain the temporal coherence of the XUV pulse train, possibly allowing it to be used for high resolution, frequency domain applications. A related benefit is the ability to study the HG process with greatly increased resolution.

In this letter, we present an experimental study of below-threshold HG by utilizing a 1070 nm ultrafast fiber laser coupled to a high repetition rate femtosecond enhancement cavity. The enhancement cavity allows us to couple a train of ultrashort pulses directly to the cavity resonance producing a large enhancement of the pulse energy and average power [12]. In our system, the laser intensity achieved at the intracavity focus is a few times 10^{13} W/cm², which is sufficient for the production of harmonics up to the 21st (near the cut-off) in a xenon gas jet [13]. Here, we concentrate on harmonics 7 through 13 which are produced near and below the ionization threshold in xenon. We find experimental evidence in the harmonic yields, spectra, and far-field distributions that these below-threshold harmonics contain multiple contributions with different intensity-dependent phases, which can interfere. Our theoretical analysis shows that one of these contributions is of multiphoton excitation

character, in agreement with widely held expectations for below-threshold HG [14]. Remarkably, we find that the other contributions have clear analogies to the semi-classical long trajectories familiar from above-threshold HG [15]. These contributions are dominated by laser-driven continuum dynamics and therefore have dipole phases which are strongly dependent on the laser intensity, in contrast to the multiphoton process. The finding of an intensity-dependent phase contribution to below-threshold harmonics opens the possibility to separately study and control the two generation mechanisms via macroscopic phase matching conditions. This could be important for the synthesization of below-threshold attosecond pulse trains.

The 1070 nm fiber laser system used in this experiment is outstanding for femtosecond enhancement cavities in that it displays both high average power and exceptional temporal coherence and frequency control, as described in [16, 17]. Briefly, a Fabry-Perot type Yb fiber oscillator operating at a center wavelength of 1070 nm is modelocked with a saturable absorber producing femtosecond pulses with 100 mW of average power. The 136 MHz pulse train is linearly amplified at the full repetition rate of the oscillator in a chirped-pulse amplifier based on cladding pumped Yb fiber. After amplification, the pulses are re-compressed to 75 fs with the resulting system displaying more than 10 W of average power.

The pulse train is actively kept on resonance with the femtosecond enhancement cavity by controlling both independent degrees of freedom of the associated frequency comb, the repetition rate and the offset frequency. On resonance, we achieve an enhancement of 260 to obtain an average intracavity power of up to 2.6 kW and an intracavity pulse duration of ~ 100 fs. The focus in our cavity is created by two 10 cm radius of curvature mirrors which produce a calculated focal spot area of 960 μm^2 and a peak intensity of 4×10^{13} W/cm². The cav-

ity acts as a mode filter, enabling a near perfect TEM₀₀ gaussian mode of the driving field. We inject xenon gas near the intracavity focus using a glass nozzle with a 100 μm aperture and a backing pressure of 425 Torr. The placement of the gas jet is estimated to be $\sim 500 \mu\text{m}$ after the focus so that the intensity in the gas is somewhat lower than the peak intensity at the focus.

To measure the harmonic power, we use an XUV diffraction grating as one element of the enhancement cavity so that a portion of the harmonic radiation will diffract out of the cavity [13]. While this technique was designed to minimize the nonlinear dispersion of the cavity, an additional benefit is that individual harmonics are easily resolved. With xenon gas injected at the intracavity focus, we are able to observe individual harmonics on a sodium salicylate plate by reimaging the fluorescence onto a CCD camera.

By varying the laser power and monitoring the fluorescent plate, we have conducted a study of the individual harmonic yields as a function of driving field intensity. In Fig. 1 we plot the on-axis yield for harmonics 7 through 13 as a function of the laser intensity at the gas jet center. The intracavity power was measured accurately for each data point by monitoring the transmitted power through one high reflector of the enhancement cavity. It is striking that the three below or at threshold harmonics (7, 9, and 11) exhibit complicated intensity-dependent yields, with steep increases interrupted by steps, rather than a perturbative power law increase. For harmonics 7 and 11 these steps are more pronounced and happen at lower intensities than for harmonics 9 and 13. The insets show experimentally measured far-field spatial profiles of each harmonic at an intensity of $2 \times 10^{13} \text{ W/cm}^2$. It is especially interesting that harmonics 7 and 11 exhibit strong off-axis halos in their spatial distributions whereas 9 and 13 do not.

To understand the observed behavior we calculate the combined microscopic-macroscopic response of the xenon gas to the 1070 nm focused laser pulse via the coupled, non-adiabatic solutions of the time-dependent Schrödinger equation (TDSE) and the Maxwell wave equation. Our implementation of the coupled solutions is described in detail in [18], with the important difference that for the work described here we are directly integrating the TDSE numerically within the single active electron approximation [19]. We are thus treating the laser electric field and the atomic potential on an equal footing which is necessary to describe harmonics with photon energies below and close to the ionization threshold. As initial conditions for the calculation we use the same parameters as the experiment [20].

As shown in Fig. 1 the comparison between theory and experiment is excellent. The theory results reproduce the overall increase of the yield with intensity and, in agreement with the experiment, exhibit prominent intensity-dependent steps in harmonics 7 and 11, and less pro-

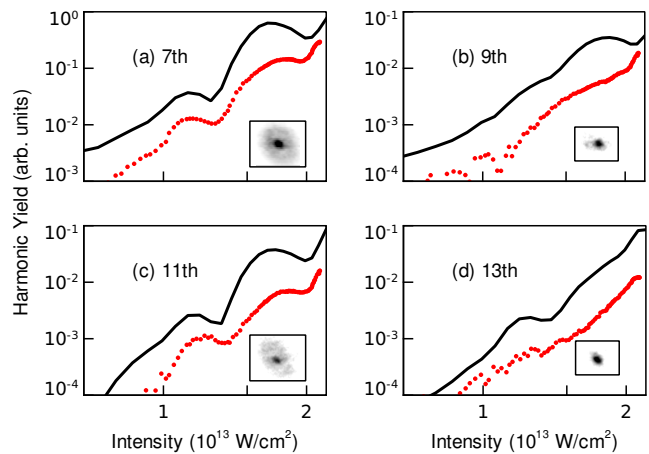


FIG. 1: (Color online) Harmonic yield plotted as a function of the intensity at the center of the xenon jet. (a)-(d) shows harmonics 7 through 13, respectively. The red data points are measured and the solid lines are theory (see text), both for the on-axis yield. Theoretical harmonic yields were scaled in magnitude to offer a clear comparison. The insets show the far-field spatial profile for each harmonic. Halos are clearly visible in harmonics 7 and 11.

nounced steps in harmonics 9 and 13. In addition, the positions of the steps are remarkably well reproduced by theory. We find that the positions of the intensity steps, as well as the overall increase with intensity, are very similar in different focusing conditions as long as we compare intensities in the gas jet and not in the laser focus. The steps are recognizable at these intensities even in the single-atom intensity-dependent dipole strength, calculated by solving the TDSE for a series of pulses with quasi-constant peak intensities [19]. This suggests that the intensity dependence of the data observed in the experiment has its origin in the strong field response at the single atom level.

To explore the origin of the steps, we analyze the single atom intensity-dependent dipole moment $d_q(I)$ for each harmonic q in terms of its conjugate phase variable α , as described below. For above-threshold harmonics the dipole moment at a given intensity can be written as a sum of a few different contributions (quantum paths) each with a characteristic phase coefficient α_j :

$$d_q(I) = \sum_j A_j e^{-i\alpha_j U_p(I)/\omega}, \quad (1)$$

where $U_p = I/4\omega^2$ is the ponderomotive energy, and ω is the laser frequency. In the semi-classical model these quantum paths are related to different electron trajectories that return with the same energy [21], and α_j is a measure of the action accumulated along trajectory j in units of U_p/ω [15]. In particular, the so-called short and long trajectories in the semi-classical model give rise to phase coefficients that are close to $\alpha_1 \approx 0.1\pi - 0.2\pi$ and $\alpha_2 \approx 2\pi$, respectively, in the harmonic plateau.

From the calculated dipole strength and phase we deduce the weight of each contribution over a range of intensities around I_0 via the transform:

$$\tilde{d}_q(\alpha) = \int d_q(I) e^{i\alpha U_p(I)/\omega} W(I - I_0) dI, \quad (2)$$

where $W(I - I_0)$ is a window function centered on I_0 [22]. For above-threshold harmonics, the phase coefficients obtained in this way correspond well to those predicted by the semi-classical model [23]. To our knowledge, this analysis has not been applied to below-threshold harmonics before.

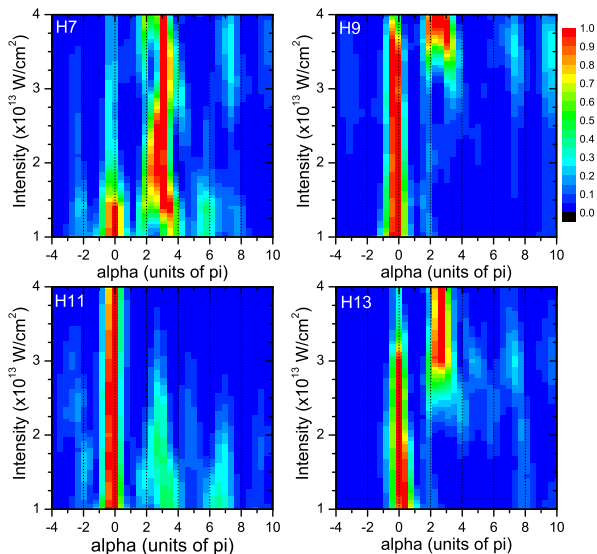


FIG. 2: (Color online) Quantum path distributions for harmonics 7, 9, 11, 13. The color scale has been normalized for each intensity and shows only relative strengths.

Fig. 2 shows the result of the quantum path analysis for harmonics 7–13 in xenon. All the harmonics exhibit multiple quantum path contributions; the two dominant ones with phase coefficients $\alpha_0 \approx 0$ and $\alpha_2 \approx 2.5\pi - 3\pi$. In the following we will argue that all the phase contributions to the below-threshold harmonics with $\alpha_2 \approx 2.5\pi - 3\pi$ and larger are analogous to the semi-classical long trajectories familiar from above-threshold generation, while the $\alpha_0 \approx 0$ contribution is due to a multiphoton excitation process that does not have a phase proportional to the laser intensity.

To understand the origin of the α_2 contribution to the below-threshold harmonics we have studied electron trajectories in a generalized semi-classical model in which the atomic potential is present. To simulate tunnel ionization we release electrons into the laser field with zero kinetic energy at the position of ionization $x_i \neq 0$, just outside the laser suppressed Coulomb barrier. We find the familiar short and long trajectories that bring the electron back to x_i with positive total energy. In fact, as

noted by Lewenstein [1], recombination and light emission take place at the ion core, and the electron can gain or lose additional energy to the laser field during the travel from x_i to the position of the core at $x = 0$. Crucially, in the presence of the atomic potential, low-energy electrons can lose enough energy to have less than zero total energy at $x = 0$, leading to the emission of below-threshold harmonics. In the tunnel ionization model, this can only happen for electrons which have followed the long trajectory because they return to x_i at a time when the force from the laser field is against their motion. There are no negative-energy returns for short-trajectory electrons in this model because they return to x_i at a time when the laser field further accelerates them toward $x = 0$. We find that the long trajectories accumulate an intensity-dependent phase which is slightly larger than in the no-potential case, with a phase coefficient close to 3π for the range of intensities we are interested in. This is in good agreement with the result in Fig. 2.

To understand the origin of the $\alpha_0 \approx 0$ phase contribution we have attempted to recover short trajectories with small phase coefficients and negative return energies by initiating electron trajectories with non-zero velocity at $x = 0$, simulating their ionization as a multiphoton process. Under the limited range of initial conditions where we do find such trajectories, their phase coefficients are also larger than in the no-potential case with $\alpha_1 \approx 0.5\pi$. Fig. 2 shows that such α_1 contributions are not present in the fully quantum mechanical results. This leads us to designate the α_0 contribution as a multiphoton process with no intensity-dependent phase, and not a generalized short trajectory dominated by laser continuum dynamics.

The analysis presented in Fig. 2 allows us to understand the experimental results in Fig. 1 as manifestations of the multiple generation mechanisms discussed above. For instance, the strong halos in the far-field spatial profiles of harmonics 7 and 11 result from the large α_2 contribution to these harmonics at intensities below 2×10^{13} W/cm². This is because the rapid dependence of the α_2 phase on intensity causes these harmonics to be generated with a phase front that is strongly curved across the diameter of the laser focus, which increases the divergence of the harmonics and gives rise to halos in the far field [24]. We see a similar effect in the spectral profile of harmonic 7 which is very broad due to the large chirp imposed by the α_2 contribution.

In addition, Fig. 2 shows that the the measured steps in the on-axis intensity-dependent yield for harmonics 7 and 11 correlate well with the intensities where there are multiple phase contributions to these harmonics. This indicates that the steps are a result of interference between the two different processes contributing to the harmonic generation. This is further demonstrated by Fig. 3 which shows experimental results for harmonics 7 and 9 in which we have separately plotted the yields in the cen-

tral spot and the halo. The steps are largely absent in the off-axis yield because the multiphoton $\alpha_0 = 0$ contribution gives rise to collimated harmonics only [25]. We also note that the abrupt appearance of a halo (and interference) at high intensity for harmonic 9 is in agreement with the theoretical prediction in Fig. 2.

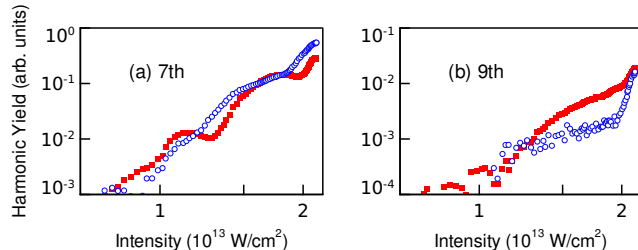


FIG. 3: (Color online) Measured intensity dependence of inner and outer parts of harmonics (a) 7 and (b) 9. Red squares show the inner portion of the beam while the blue open circles show the outer portion. While the outer part of the beam is dominated by the α_2 contribution, the central part of the beam contains contributions from both α_0 and α_2 .

Finally, Fig. 3 suggests that phase matching may be used to separately study and control the multiphoton and semi-classical contributions to the below-threshold harmonics. We expect that the multiphoton contribution, with a phase which depends only weakly on intensity, will be relatively insensitive to the geometrical phase matching configuration compared to the semi-classical contribution. Moving the focus relative to the gas jet will therefore change the relative strengths of the two contributions, in analogy with above-threshold HG. In particular, to isolate the multiphoton contribution we propose to move the laser focus downstream from the gas jet which will minimize on-axis phase matching for the semi-classical contribution [26]. Our calculations show a pronounced reduction in the interference effects in the on-axis yield in this configuration, indicating that a spatial filter could select one contribution or the other.

In summary we have found experimental and theoretical evidence for multiple contributions to the generation of below-threshold harmonics in xenon. In particular, one of these contributions is dominated by laser-driven continuum dynamics, in analogy with the semi-classical model for generation of high order harmonics. The prospects of using phase matching to manipulate these low order harmonics is exciting for frequency domain applications requiring a precise frequency comb in the XUV, as it would allow us to select the temporally coherent portion of the beam, dominated by an α_0 which may be truly zero. More generally, understanding the generation mechanisms for below-threshold harmonics, which have much higher conversion efficiencies than harmonics high above threshold, is critical for future work with high repetition rate HHG.

We gratefully thank I. Hartl, A. Marcinkevičius and M. Fermann at IMRA America, Inc. for the design and construction of the high-power Yb-fiber laser system. Funding at JILA is provided by DARPA, NIST and NSF. This material is based upon work supported by the National Science Foundation through grants number PHY-0449235 and PHY-0701372, and by the Center for Computation and Technology at Louisiana State University. KJS acknowledges support from the Ball Family Professorship.

-
- [1] M. Lewenstein, P. Balcou, M. Y. Ivanov, A. L’Huillier, and P. B. Corkum, *Phys. Rev. A* **49**, 2117 (1994).
 - [2] M. Meckel *et al.*, *Science* **320**, 1478 (2008).
 - [3] M. Hentschel *et al.*, *Nature* **414**, 509 (2001).
 - [4] G. Sansone *et al.*, *Science* **314**, 443 (2006).
 - [5] S. T. Cundiff and J. Ye, *Rev. Mod. Phys.* **75**, 325 (2003).
 - [6] T. Udem, R. Holzwarth, and T. W. Hänsch, *Nature* **416**, 233 (2002).
 - [7] A. Marian, M. C. Stowe, J. R. Lawall, D. Felinto, and J. Ye, *Science* **306**, 2063 (2004).
 - [8] E. E. Eyler *et al.*, *Eur. Phys. J. D.* **48**, 43 (2008).
 - [9] S. Witte *et al.*, *Science* **307**, 400 (2005).
 - [10] R. J. Jones, K. D. Moll, M. J. Thorpe, and J. Ye, *Phys. Rev. Lett.* **94**, 193201 (2005).
 - [11] C. Gohle *et al.*, *Nature* **436**, 234 (2005).
 - [12] R. J. Jones and J. Ye, *Opt. Lett.* **29**, 2812 (2004).
 - [13] D. C. Yost, T. R. Schibli, and J. Ye, *Opt. Lett.* **33**, 1099 (2008).
 - [14] For example, an earlier theoretical study in potassium found below-threshold harmonic generation to be profoundly influenced by three and five photon $4s-4p$ resonances. M. B. Gaarde and K. J. Schafer, *Phys. Rev. A* **64**, 013820 (2001).
 - [15] M. Lewenstein, P. Salières, and A. L’Huillier, *Phys. Rev. A* **52**, 4747 (1995).
 - [16] I. Hartl *et al.*, *Opt. Lett.* **32**, 2870 (2007).
 - [17] T. R. Schibli *et al.*, *Nature Photonics* **2**, 355 (2008).
 - [18] M. B. Gaarde, J. L. Tate, and K. J. Schafer, *J. Phys. B* **41**, 132001 (2008).
 - [19] K. J. Schafer and K. C. Kulander, *Phys. Rev. Lett.* **78**, 638 (1997).
 - [20] The calculations are performed with 50 fs pulses to save computing time. We have checked that the results do not change for longer pulses.
 - [21] K. J. Schafer, B. Yang, L. F. DiMauro, and K. C. Kulander, *Phys. Rev. Lett.* **70**, 1599 (1993), and P. B. Corkum, *Phys. Rev. Lett.* **71**, 1994 (1993).
 - [22] Ph. Balcou *et al.*, *J. Phys. B* **32**, 2973 (1999).
 - [23] M. B. Gaarde and K. J. Schafer, *Phys. Rev. A* **65**, 031406(R) (2002).
 - [24] M. Bellini *et al.*, *Phys. Rev. Lett.* **81**, 297 (1998).
 - [25] Interference in yield between different tunneling contributions has been observed far off-axis for above-threshold harmonics, where the long-trajectory contribution is much weaker than the short-trajectory contribution, see A. Zair *et al.*, *Phys. Rev. Lett.* **100**, 143902 (2008).
 - [26] P. Salières, A. L’Huillier, and M. Lewenstein, *Phys. Rev. Lett.* **74**, 3776 (1995).